33RD CONGRESS
OF THE INTERNATIONAL COUNCIL
OF THE AERONAUTICAL SCIENCES
STOCKHOLM, SWEDEN, 4-9 SEPTEMBER, 2022

ICAS 2022 SWEDEN

Analysis and Development of Integrated Low-Pressure Shaft Generator

Avo Reinap[1], Magnus Genrup[2], Richard Avellán[3], Hans Mårtensson[3]

[1] Div. Industrial Electrical Engineering and Automation,
Lund University, Box 118, 221 00 LUND, Sweden
[2] Dept. Energy Sciences, Lund University, Box 118, 221 00 LUND, Sweden
[3] GKN Aerospace, Sweden

Abstract

The work focuses on analysis and development of integrated low-pressure shaft generator in a geared twin-spool turbofan engine. It starts with manufacturing and evaluation of direct cooled hollow conductor coils, and has focus manufacturing, assembling and integration issues essential to machine design. The experiment-in-loop, but the model-based evaluation focuses not only on the coolant and cooling system study and on the characterization of the electric machine, but also when exploring the additional design issues related to electric drive systems for permanent magnet synchronous machines and studying the features of power transfer between the turbo engine spools.

Keywords: Design of electrical machines, Direct cooled windings, Aircraft generators, Numeric field computation, Experiment oriented design

1. Introduction

Electrification of transport offers hope for more environmentally friendly and fuel-efficient transport systems and anticipation for more efficient and energy-intensive technological solutions, not just for electrical machinery but to all electrified powertrain components. The transport electrification targets for aviation in terms of increasing specific power do not leave much room for imagination when choosing traditional solutions for electrical machines integrated on the low-pressure shaft of a geared twin-spool turbofan. The use of permanent magnets and direct-cooled hollow winding is expected to increase both specific torque and power, but the relatively large shaft diameter forces a choice between a larger machine or a higher operating frequency, which inevitably results in higher power losses.

1.1 Turbine Integrated Generators

Typically, electric machines are connected to turbine engines by means of a radial transmission and an auxiliary gearbox, which also makes it possible to reduce the size of electric machines at the appropriate selection of speed and power. The history has shown the most viable, survivable rational integration of electrical machine, which is a wound field synchronous generator (WFSG), into aircraft power plant via a radial tower that not only extracts power from the high-pressure spool (HPS) but also can contribute to the start of the engine [1]. This paper reveals that even power electronics (PE) plays an ever-increasing role in the aviation industry, as in many others, there is no known commercial aircraft that until now has implemented permanent magnet (PM) or switched reluctance (SR) generator as the main electrical source, despite the perceived advantages offered by these technologies. Reference [2] gives a brief and detailed overview of the different types of electric machine topologies [2] with a view to integrating them into the HPS of the turbomachine. The preferred candidate is the FWSG, but the document does not aim to develop a more accurate cooling system for the proposed machine in this context. Articles [3]-[5] describe the development and testing of a SR machine with a *12/8 pole* topology and its converter. In addition to oil-cooled hollow conductors, the stator housing and rotor can be also directly cooled. Hollow conductors result

a low number of turns, and that due to relatively large conductor's cavity, so that more efficient fluid circulation is possible. On contrary, the large cross-section causes higher induced losses, for example when the machine is supplied at *900 Hz*, which is close to ground idle speed. Despite successful engineering and testing, there, according to authors is some space for efficiency improvement, which is measured *85%* at half load.

The addition of an LP shaft generator often requires that this machine operate only at the generator mode and over a wide range of speeds. Articles [6]-[8] give a good overview and experience of the search, design and testing of solutions where a *5-phase* machine with an internal stator diameter of *350 mm* must be able to operate at electrical frequencies of *245-723 Hz*. Experimentally, the machine allows an efficiency of more than *90%* over wide output range, the short-circuit current value is not higher than the rated current but it causes a large torque ripple and destabilization power swing. There are several challenges for direct-connected electrical machines, and when looking at the direct connection options of the LPS, there is a first-hand direct challenge to the size of the shaft, the speed range, and the reliability requirements for the electric power generation.

1.2 Machine Concept Selection

While PM-type machines are almost excluded from the list of generators practically used in larger commercial aircraft, PM motors are a reality for smaller electric aircraft. Among them are machines that are a good example in terms of size, power, speed, frequency, and viable PE solutions [9]. The size of the permanent magnet synchronous machine (PMSM) under investigation is shown in Figure 1 and different topologies are compared in [10].

- Stator topologies: a fractional slot concentrated winding (*FSCW*) and a distributed winding (DW) where the slots can be formed differently depending upon which conductors are used and how they are inserted into the slots
- Rotor topologies: a Halbach-type magnet arrangement (*HAPM*) and an interior permanent magnet (IPM) rotor

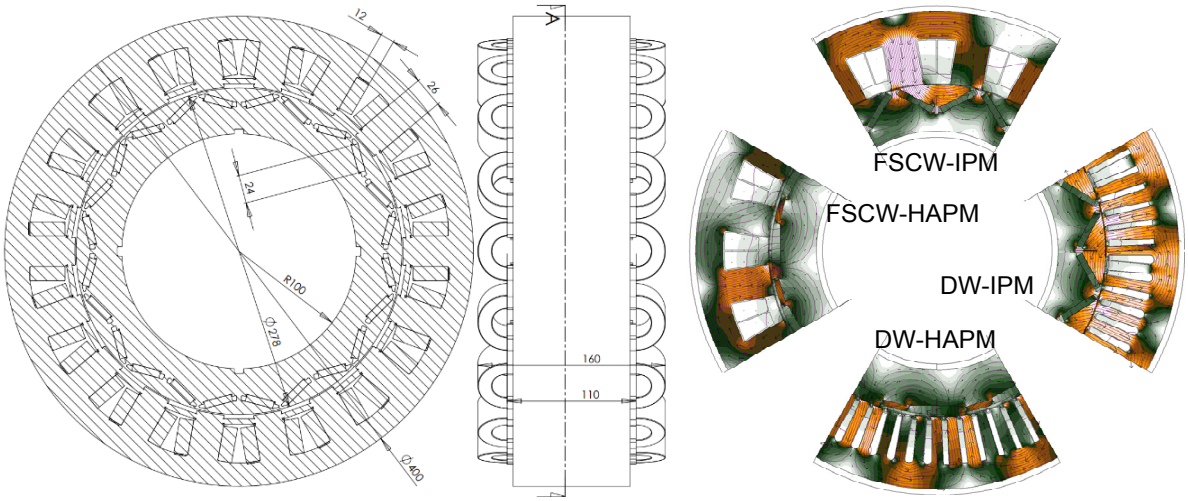

Figure 1 – The preferred machine layout (left) and the flux density distribution (color scale from 0 to 2 T) of design candidates

Figure 1 shows the construction of the machine as the initial preference, which allows easy assembly of prefabricated coils and the nonoverlapped coils are more suited for fault tolerant operation. One of the topics of interest is the design of hollow conductor coil and this not only in the electrical and hydraulic termination point of view but more generally when examining, cooling and winding arrangement together with converter topologies for more efficient extraction of electric power over the wide speed range. From thermal management point of view, it is important that the choice of coolant, required flow rate and pressure head provides a rational and reliable solution.

1.3 Cooling Integration

The cooling principles for electric machines can be divided not only between active and passive cooling methods, but also according to the proximity of the cooling circuits to heat sources based on how cooling integration is performed (Figure 2).

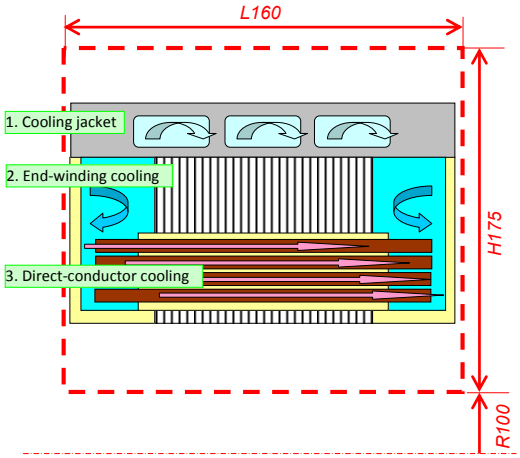

Figure 2 – Radial-axial planar cross-section of an electric machine stator showing basic cooling methods as well as geometric constrains

The cooling integration and thermal management of the stator relies on a distributed stator core cooling jacket and direct cooling of concentrated windings. The topological preference of the electrical machine under study is based not only on the modularity and redundancy of the winding, but also on the experiments being developed and studied, which allow immediate monitoring and model-based evaluation of component performance, productivity and assembling challenges.

The thermal management system becomes inevitable for a high power-density system and its efficiency depends on the cooling integration. Decades-old cooling solutions, tests and the resulting trends in aircraft generators are not only inspiring but also up to date [11]. This 1970 article summarizes the experimental evaluation of a 63kVA three-stage FWSG using an indirect oil-cooled machine and a direct-spray-cooled machine. As concerns about moving the coolant closer to or inside the conductor focus on the following paper. The use of hollow conductors is attractive because they offer a direct cooling option, as shown in [12] by the satisfactory results of a high power (*300 kW*) medium frequency (*5 kHz*) transformer using large rectangular hollow wires (*1.5 mm thick*) that showed less concern on induced losses.

2. Direct Cooled Windings

Direct-cooled windings are defined here as live conductors that have direct contact with the coolant to directly divert the generated Joule losses from the windings. There are many examples where the power of a machine is literally doubled by replacing indirect-cooled windings with direct-cooled windings an example given by the hollow conductor manufacturer [13] and system developer [14]. The number of practical challenges will increase not only as the system is integrated, but also as it becomes more compact and powerful. An example of the pressures and flows in [14] as documented: *30 bar 1.4 L/min*, *50 bar 1.8 L/min*, *70 bar L/min* using heat transfer oil which indicates the challenges of using a hollow conductor as a cooling system.

2.1 Winding Layout Specification

The main purpose in defining direct-cooled coils and windings lies with the existing hollow conductors, which allow test specimens to be prepared and developed. This condition affects not only the design choices and dimensions, but also the winding connections and the rated voltage of the machine.

In fact, completing the high-pressure termination of the hollow conductor to the pump circuit is usually a discarded detail at the beginning of the experimental design as the main goal is to have a high coil filling factor in the stator slots for purpose of less heat generation and better heat dissipation. However, a round tube is easier to connect to the pump system than rectangular. In addition, since aeronautical electrical machines are likely to operate in the range of *0.5* to *1 kHz*, where Litz wire is a good alternative to an almost solid conductor such as a larger size hollow conductor. Article [15] gives a good example of a *7.6 x 8 mm* Litz wire consisting of *8 bundles* with *24 strands* each around a cooling tube made of steel, which is in the middle of the conductor. The inner and outer diameter of the pipe is *3* and *4 mm*, respectively. A *5.1 m* wire is used for the *8-turn* test coil that is part of a *12-slot*, *8-pole* FSCW IPM machine. The water-cooled system pressure is *6 bar* for a flow rate of *2 L/min* and *135 W* (173 ADC) of heating power was used for experimental

validation of the 3D Comsol Multiphysics models. This is an example with a practical approach to understanding the multidisciplinarity of the coil design and cooling integration.

2.2 Concentrated Windings

The advantage of concentrated windings is that the heads of the coils do not overlap and selecting open-slot stators facilitates reliability and a parallel electrical machine manufacturing process. The coils used in the winding are identical or divided into two groups, which allows a higher filling factor in the stator slots. Figure 3 shows the cross-section and arrangement of the windings on the two stator teeth and the adjacent CAD shows the stator components assembled.

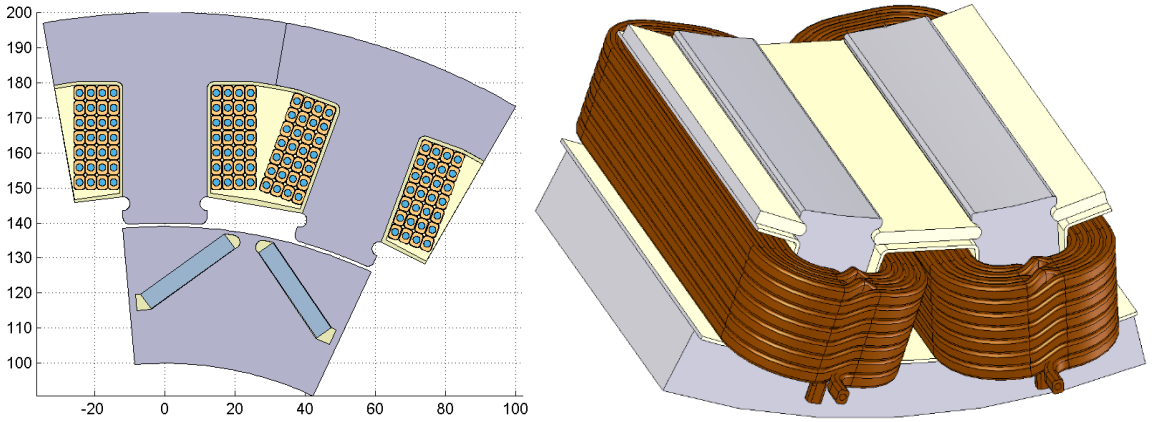

Figure 3 – A fraction of stator assembly consisting of two coils:
2D cross-section including rotor(left) and 3D image

2.3 Distributed Windings

Distributed windings have a wider winding pitch, higher winding factor, and thus lower harmonic content and ripple than concentrated windings, but as the winding heads must overlap, the heads become long, with additional power losses in the end turns, and require more space. By choosing the Luvata *3x4ø2 mm* hollow conductor, one can also get a more detailed image of the arrangement of the conductors of DW (Figure 1) in the stator slots (Figure 4). The stator slot is semi open which means that the windings are inserted axially as segmented bar shaped windings [16] instead of being inserted radially which allows for continuous wire [17]. The first solution allows for parallel coil cooling, pressure and higher flow rates while creating challenges in collecting leak flows [18].

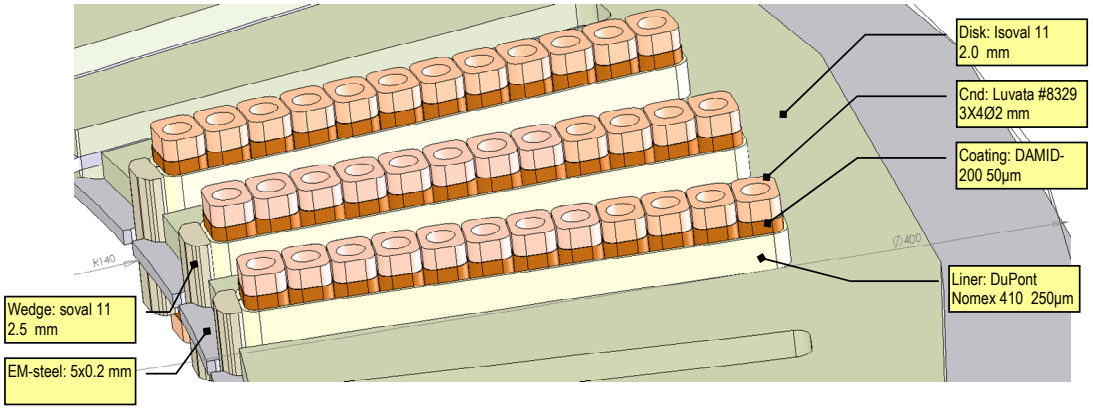

Figure 4 – Detailed view of components assembled in 72-slot DW stator

3. Prototype Coils

Developmental experimental testing begins with the production of test coils, focusing on two different production methods. This is followed by the development of a cooling system and its evaluation system, and it starts with three different coolants: air, dielectric mineral oil and water. The experiential detail-based skills are required for the further development of electrical machine design towards higher reliability and loads.

3.1 Coil Design

The design and formation of the winding is analyzed using 3D geometric modeling software to deepen the mathematical formulation and geometric formation of the coil, especially the transition of the end turn in crossover section. A design table in SolidWorks is used to define the hollow conductor coil. The base structure (Figure 5) is defined by using a c-shaped path for a coil turn at the same working plane and a cross-section of the hollow conductor, which includes the enamel insulation.

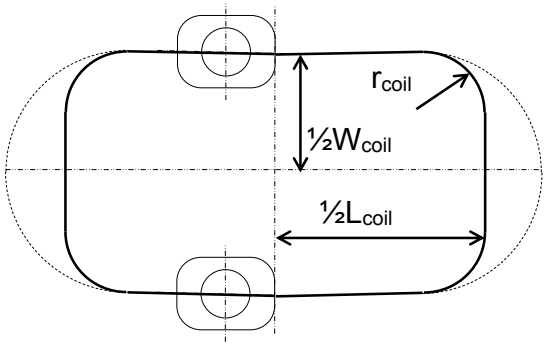

Figure 5 – Hollow conductor coil parameterization

The coil specification is following:

1) The cross-section of the hollow conductor: is defined by the height h_{hc}=*4.1 mm* and the width w_{hc}=*3.1 mm* of the "standing" wire. The inner hollow diameter is d_{hc}=*2 mm* and the corner radius is defined r_{hc}=*0.85 mm*.
2) The c-shaped path for the coil turn: is the base structure for the remaining turns and layers, and defined as follows.
   a. Coil width W_{coil}: is attached in the middle of coil and not to the interior or exterior width of the specific layer.
   b. Coil length L_{coil}: considers only the straight path of the wire in the stator slot and the extension from both ends of the stator stack. For the given stator stack of *100 mm* and the extensions of *5 mm* results L_{coil}=*110 mm*.
   c. Coil radius r_{coil}: grows with each succeeding layer N_{layer} and is limited by the smallest bending radius for the hollow conductor. The largest radius $r_{coil.max}$ is defined (1) by the (minimum) stator tooth width w_{st}=*24 mm* and where the insulation liner thickness w_{ins}=*1 mm*.

$$r_{coil.max}=½(w_{st}+2w_{ins}+w_{hc}+2(N_{layer}-1)\,w_{hc}) \qquad (1)$$

Table 1 – Coil layer specifications

Layer N_{layer}	Dimensions [in mm], resistance and power losses					
	½w_coil	*r_coil*	*1 turn*	*7 turns*	*R_coil[mΩ]*	*P_coil[W]*[b]
1	14.6	10.0	364	2548	8.93	357
2	17.7	13.1	403	2821	9.89	396
3	20.8	16.2	442	3094	10.86	434
4	23.9	19.3	481	3367	11.82	473

[a.] Resistance calculated at 120°C and resistive power losses at 200A

If the specified coil (in Table 1) would result in wire length of *11.83 m*, DC resistance *41.7 mΩ* and power losses *1.66 kW* at *120°C* and *200 A* (*29.2A/mm²*) then smaller radius r_{coil}=*3 mm* at the first layer reduces resistance to *36.0 mΩ* and the total (axial) coil length becomes *140.8 mm* instead of *154.8 mm*. The larger radius of r_{coil}=*14.5 mm* at the first layer increases DC resistance to *45.7 mΩ* and the coil length to *163.8 mm*, respectively. This comparison does not include the additional length due to cumulation of tolerances, transitions between layers and levels and prolongations to the termination points.

In this work, the focus is on two hollow coils: 4- and 28-turn, where the former uses about 10% wire compared to the latter. Figure 6 shows not only the dimensions taken in top view, but also pays

attention to the importance of forming the end turns of the crossover sections. The upper figure demonstrates a smooth transition of half a turn, which results in a slope or inclination when the turn is not twisted backwards. The bottom figure shows the formation in two parts, using a separate work plane at the same time. The red colored inspection measures are used to connect information in Table 1, Figure 6 and Figure 7.

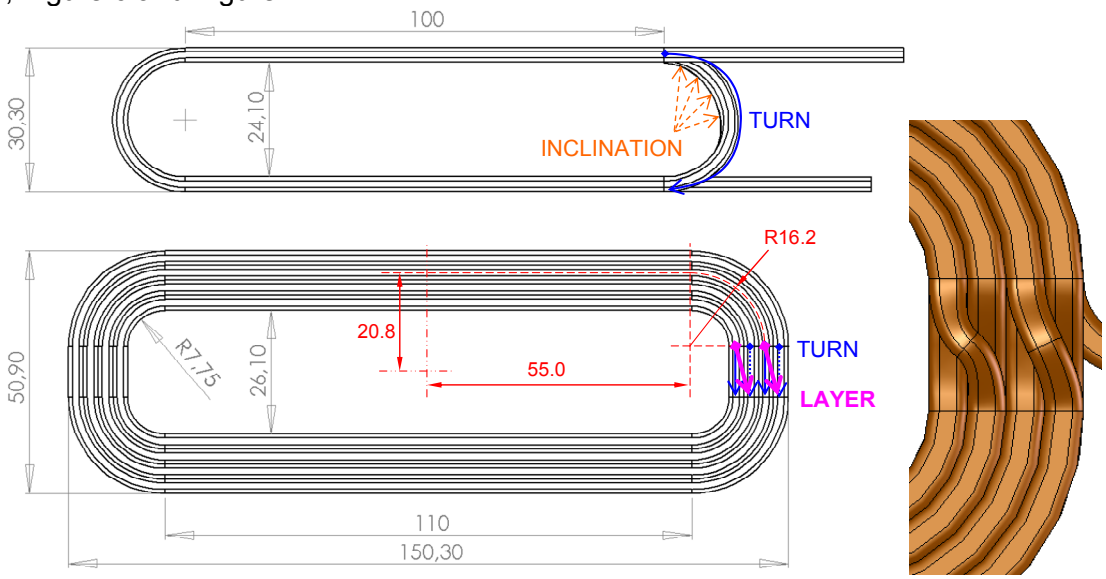

Figure 6 – Top view according to the technical drawings of the coils: 4-turn above and 28-turn coil in the bottom. The detailed image on the right shows the transitions of the winding layers where different transition angles have been used as acompromise between a shaper bend and incrusion

3.2 Prototyping Evaluation

The coil is made by hand, taking advantage of the wooden bobbin for protecting insulation enamel when forcing, forming, and packing the wire into the coil. The wire with a rectangular cross-section is straightened and positioned so that the wider side of the wire is against the workbench. The source end is secured, and the mechanically tensioned wire is wound on the bobbin. When making the coil, care must be taken that the wire would not twist when forming end-turn, starting new turn or layer that would result unnecessary deviation or inclination that is shown in Figure 6 and Figure 7.

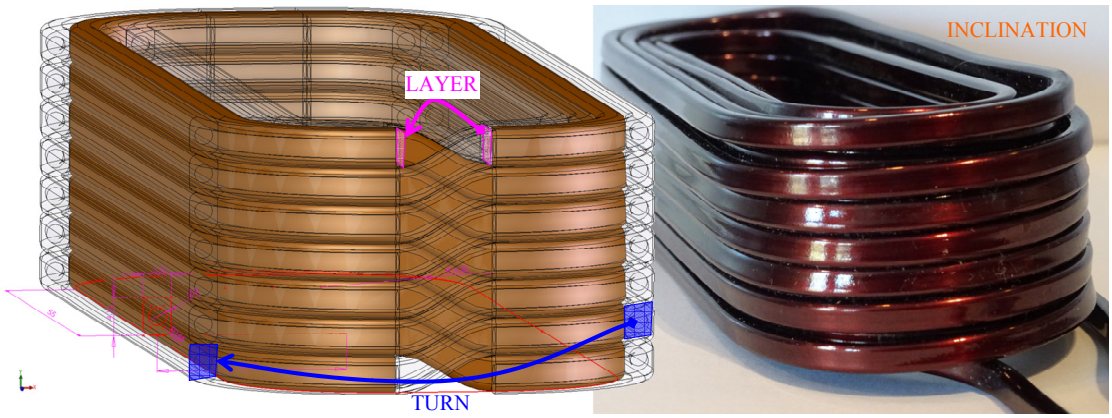

Figure 7 – The wire transition of the end turn in crossover section in the terminal end accoring to geometric modeller (left) and fabricated coil (right).

In the production of the 28-turn coil, the first production method chosen is the stepwise transition in the cross-section. The purpose of this method is to distinguish two different deformations: 1) the bend r_{coil}, and 2) the twist between the turns. The focus of the method is on fixing the wire and forming the end turns of the coil head in the crossover section. As the winding wire goes from the lower layer to the top, the formation of a step and twist while keeping the winding wire under moderate mechanical tension, gives less accurate results than winding the coils under tension and then compressing the turns and layers to the desired dimensions. Thus, the second manufacturing method can be described as a smooth and compressed transition in the crossover section of the end turn. The main concern in the manufacture of coil is not the recoil or the displacement due to

the reaction forces, but the control of the forces applied to form the turns and the natural or easily occurring direction of the materials. This leads to inaccuracies and cumulative discrepancies. However, this is a good experience for more accurate model-based monitoring of coil production and selection of the appropriate manufacturing technology [19].

The dimensions LxWxH of the coil bobbin are *119x25x29 [mm]* and are deliberately chosen to account for the wire displacement due to reaction forces even when the wire is regularly forced to take the desired position through manufacturing process. The dimensions *LxWxH* of the coil interior opening are *120x26x30* and the length *L* and width *W* of the outer sides are *148* and *53.5* mm, respectively. Even if the width between the inner sides of the coil is the same as the width of the insulated stator tooth (Figure 1), and that at a given measurement accuracy, the winding is sufficiently deformable to place it on top of tooth and insulation and slide it into the slot. A major concern is that the width of the outer sides of the coils is *2.4 mm* wider and there is less space between the corners of the coils. In the manufacture of the winding, it is already assumed that the front of the winding, and in particular the terminal side, grows geometrically, and this has also been considered in the choice of corner radii, which have been reduced by a millimeter.

3.3 Cooling Evaluation

Thermal tests are performed using a previously adapted air-cooled test coil testing platform consisting of a a low voltage transformer as the heat source to provide current above *500A ac* (depending on voltage need) and various cooling devices from compressors to blowers covering the flow rate from *170* to *1700 L/min*. *Agilent 34972A* data logger is used to record temperatures from *J* and *K* thermocouples, pressure from *Gems 350050016A05* pressure transmitter (max *16 bar*), flow rate from *Sonoair VPF-R200-M100* flow meter (up *200 m^3/h* and max *16 bar*), current from *Fluke 80i-1000s* Clamp-on AC Current Probe and coil terminal voltage.

For oil cooling tests, a test bench made for electrical machines is used, the components of which were a pump: *Marco UP3* OIL Gear Pump *5.5 L/min @ Ø13mm, 2 Bar, 12V*, and a flow meter: *IR-Opflow type 04* that can measure from *1* to *30 L/min* maximum at *10 bar*. For coolants, the experiment is limited to one type of oil *Transformer Insulating Fluid MIDEL eN 1204* (fire point >300ºC).

The components of the test system described above are rather dimensioned for low pressure tests and are not suitable for characterizing low flowrates in the test specimens. As a result, tests on the water coolant have been limited to taking up the hydraulic characteristics of the test coils.

3.3.1 Air-Cooled Coils

Air-cooled experiments have been performed with both test coils, with an example of a 4-coil coil test shown in Figure 8 on the left and in Figure 9, and an example of a 28-coil coil test shown in Figure 8 on the right and Figure 10. Images from the IR camera are taken just before the heating power is turned off.

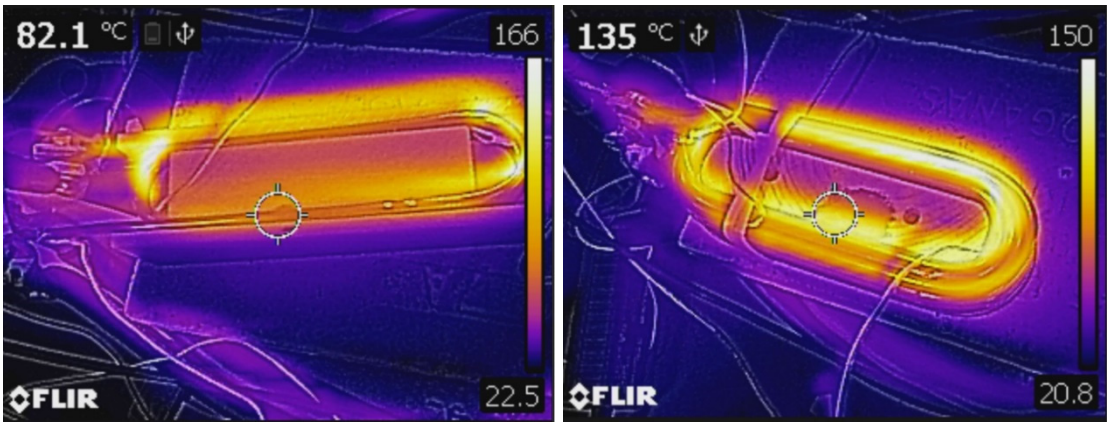

Figure 8 – Thermal images of the air-cooled 4-turn (left) and 28-turn (right) coils

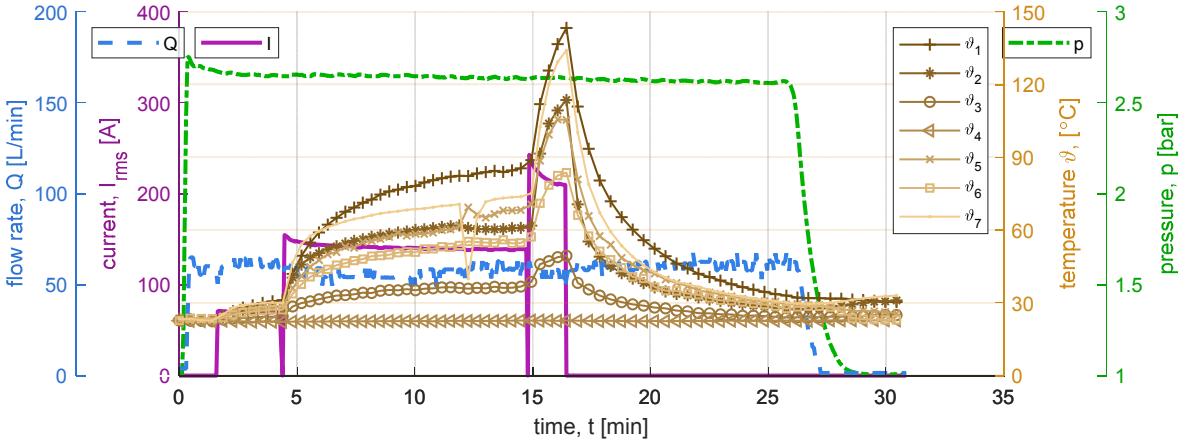

Figure 9 – flow rate (Q), current (I), temperatures (ϑ) and pressure (p) profiles of a 4-turn test coil

The recorded temperatures ϑ are: 1, 3 – coil terminal, 2 – coil body surface, 4 – near ambient temperature, 5 – outlet temperature, 7 – sensor placed between end turns (Figure 9). The purpose of the test is to evaluate the heat transient at *70*, *140* and *210 A*. The cooling flow is on average *57 L/min* and the pressure is just over *2.6 bar*. From the point of view of cooling topology, it is suitable to compare the above experiment with an identical but parallel-cooled coil where about *300 L/m*in @ *2 bar* can cool *350 A* and keep the coil temperature below *200°C [20]*.

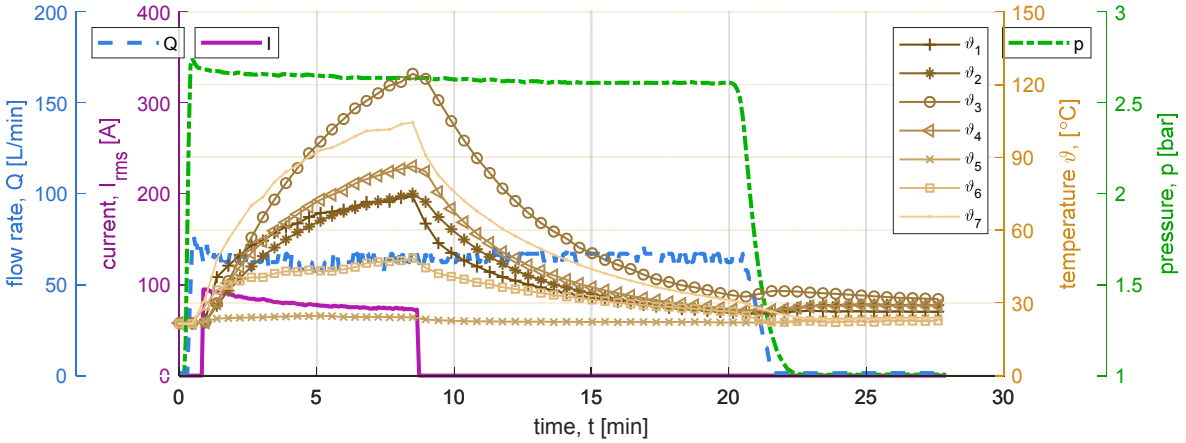

Figure 10 – flow rate (Q), current (I), temperatures (ϑ) and pressure (p) profiles of a 28-turn test coil

The recorded temperatures ϑ are: 1, 5 – coil terminals, 2, 4 – coil body surface, 3 – sensor placed inside end turns, 7 – outlet temperature (Figure 10). Compared to thermocouples the IR camera shows slightly higher temperatures. The current pulse is *8 minutes* long, starting at *95 A* and ending at *72 A*. the air cooling is limited to a pressure of *2.7 bar* at the beginning and *2.6 bar* at the end of the test and a flow rate between *62* and *67 L/min*. When evaluating the temperature transient, considering the active internal cooling and passive exterior cooling of the current conductor under these cooling conditions, then the winding allows to carry up to *70 A* which allows the continuous operation at the maximum allowable insulation temperature.

3.3.2 Oil-Cooled Coils

Oil-cooled experiments have been performed only with a 4-turn coil test, which is shown in Figure 11 and in Figure 12. The reason why the oil cooling experiments are limited to only one test piece is mainly related to the low-pressure components used in the experiment which are not able to ensure the desired coolant supply.

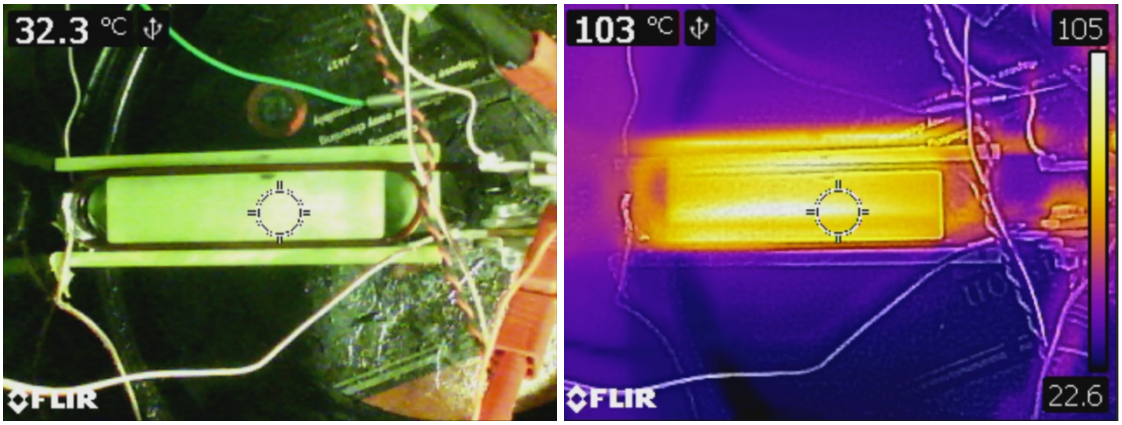

Figure 11 - Images of the oil-cooled 4-turn coil

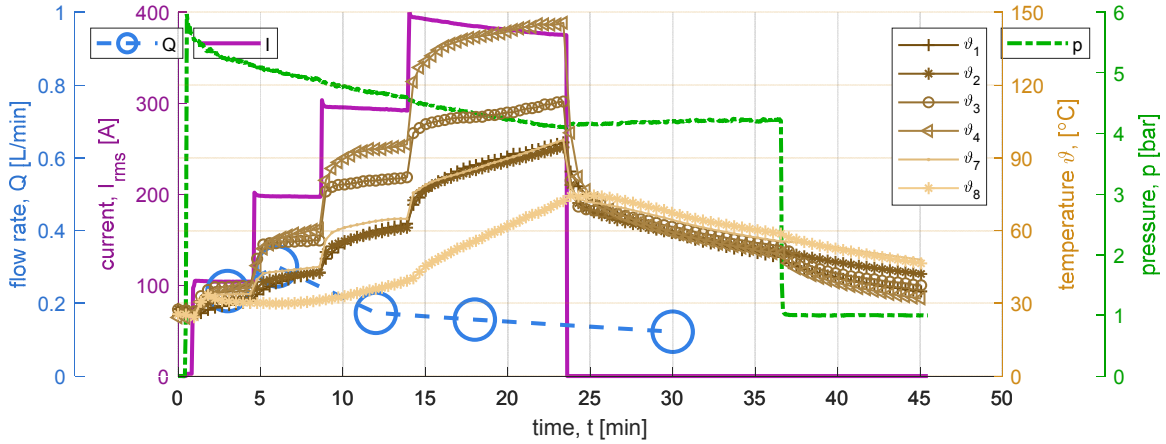

Figure 12 – flow rate (Q), current (I), temperatures (ϑ) and pressure (p) profiles of a 4-turn test coil

The recorded temperatures ϑ are: *1, 5* – coil terminals, *2, 4* – coil body surface, *3* – sensor placed inside end turns, *7* – outlet temperature, *8* – inlet temperature. the temperature profiles are directly related to the heating of the coolant in the system and this in turn affects the viscosity of the fluid. The inlet pressure starts at *6 bar* and ends at *4.1 bar* when the current is switched off. Until the circulation is switched off, the pressure rises to *4.2 bar*. The flow measurement is made by counting the flow meter pulses, whereas the normal measuring range starting at *1 L/min*. The current values are *100, 200, 300* and *400 A* or a few amps below as shown in Figure 12.

3.3.3 Water-Cooled Coils

There are some limitations to recording the hydraulic characteristics: the water pressure is less than 5 bar, the pressure can vary with the time of the measurement results, and a water level gauge is used to measure the small flowrates.

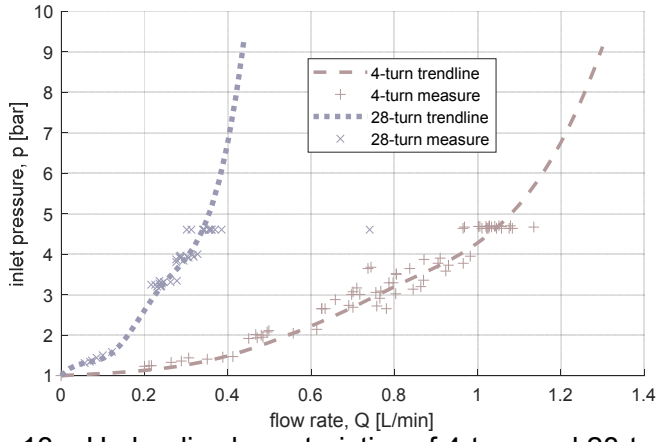

Figure 13 – Hydraulic characteristics of 4-turn and 28-turn coil

Comparing the test results of the oil-cooled system (Figure 12) with the hydraulic characteristics of 4-turn coil, water cooling allows higher flowrates at lower pressures, even with a 28-turn test coil

(Figure 13). This characterization provides a good goal that cooling will be sufficient for low viscosity and high heat capacity coolants such as water.

3.3.4 Evaluation Models

Two types of evaluation models have been developed to analyze the experiment and to compare other types of coolants. However, it should be noted that the applied comparison of coolants is limited to the availability of physical parameters of the fluid data. The purpose of hollow conductor is to provide immediate cooling and thereby control coil temperature. The cooling performance evaluation is based to a thermal liquid model, where the main components are mass flow rate and heat sources, and a segmented pipe model (Figure 14).

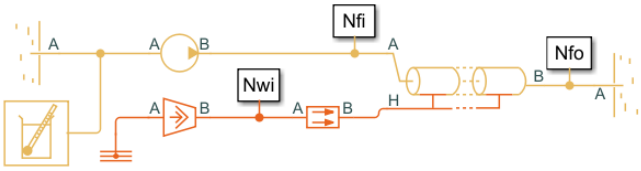

Figure 14 – Matlab Simscape thermal liquid model

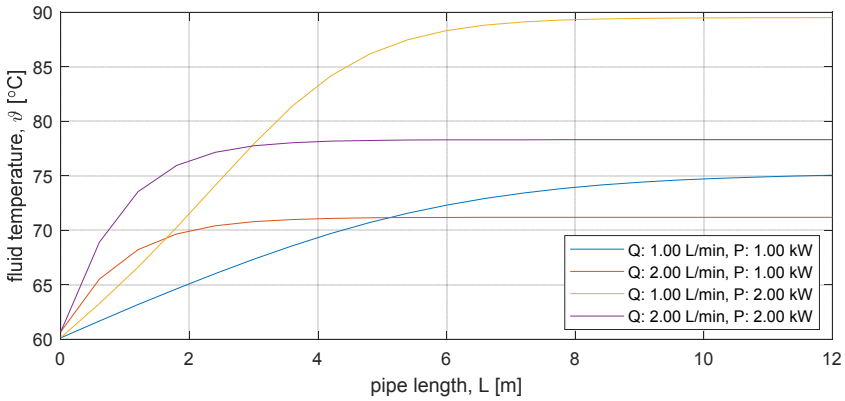

Figure 15 – Fluid temperature along pipeline

Figure 15 shows fluid temperature development along the *12 m* hollow conductor. The reference heat losses in the coil are *1.66 kW* (Table 1) and the figure gives a range of losses and coolant flow rates. Water has been used as the coolant in this calculation and the estimated internal pressure difference is *29* and *166 bar* at a flow rate of *1* and *2 L/min* at *1 kW* heating, respectively. Similar 3D conjugate heat transfer model that includes 3D pipe model is developed under Comsol Multiphysics (Figure 16) with the difference that it includes also heat transfer model for solids where the internal thermal resistance between the conductors and coil cooling surfaces are considered.

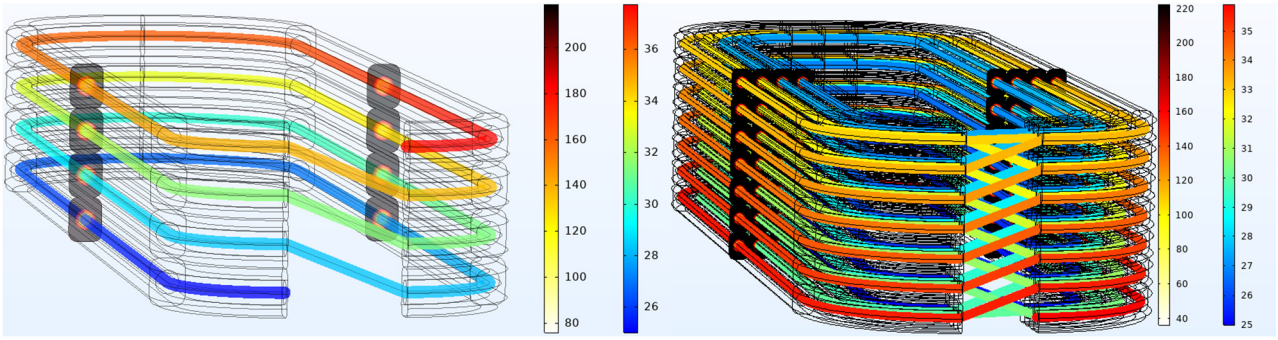

Figure 16 – Fluid temperature along pipeline and coil temperature range of the coils at 137A (20A/mm^2). 4-turn coil (left) is cooled by transformer oil (0.2 L/min) and 28-turn coil is cooled by water (1 L/min) where the inlet pressure is 2.2 and 20.4 bar, respectively.

The purpose of the simulation on the left (Figure 16) is to better understand the test results (Figure 12), but the coolant oil in the model is different from the one used in the tests and the coil temperature is also much higher than what was measured. A heat transfer factor of *10* and *1 W/m^{2}K* are added to outer surfaces of both models, the left and right images respectively, and this has a greater effect on the coil temperature compared to changing the internal thermal resistance of the coil.

3.4 Coreless Coil Parameters

The frequency characteristics of the coils are of interest in determining AC losses. Measurements have been performed on coreless coils only. The characteristics are shown in Figure 17 where the measurement number *1* belongs to *4-turn* and number *2* to *28-turn* coil. The inductance and resistance of the coils at *173.7 Hz* and *1.7 kHz* are *1.6-1.5 µH 3.26-3.52 mΩ* and *62.9-61.2 µH 21.1-60.3 mΩ*, respectively. Measurements have been made at room temperature *20°C.*

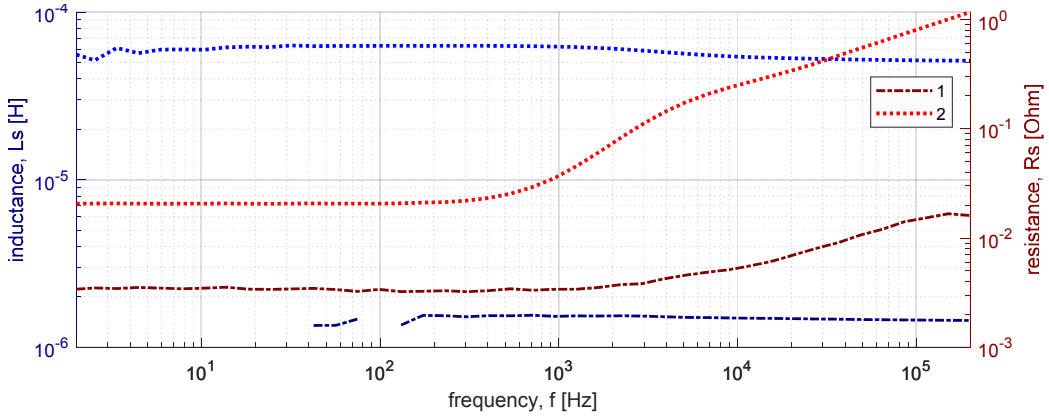

Figure 17 – *4-turn* (1) and *28-turn* (2) coil frequency dependent inductance and resistance

4. Machine Characteristics

Research and evaluation are not limited to coolant/material selection or production and electrical machine components, but also to their integration into a turbojet engine and connection to the electrical system. The latter is assessed not only in the context of heavy-duty machinery, drives and control systems, but also in terms of the challenges facing the aeronautical electrical machinery and drives. The primary interest in this section is qualitative parameters of the proposed machine topology and model-based prediction of machine characteristics.

4.1 Fractional Slot Concentrated Winding Machines

When [21] identified a direct cooled hollow conductor coil in a *FSCW* as an attractive prospect due to the cooling integration and the faultlessness design options due to dispersed insulation system and converter topology arrangements, then the initial study revealed concerns for high harmonic content. When investigating *FSCW* machines, Table 2. provides a comparison with HAPM and IPM rotor and a sensitivity study with a larger rotor bridge thickness and a larger air gap [21], resulting the same magnetic air-gap for *HAPM* and *IPM* machines. The retaining sleeve or banding is defined as the "bridge" of the *HAPM* machine, and in this comparison, two different stator materials are selected, indicating less importance of different magnetic properties, and stacking factors. The no-load phase voltage of the machine and its total harmonic distortion (*THD*) are shown in the table below. The design name begins with the type of rotor and is followed by the size of the mechanical air gap, the thickness of the bridge or retaining sleeve and the type of steel used in the stator.

Table 2 – Induced voltage comparison of FSCW machines

Design	Dimensions [in mm], voltage [V], THD [%] and torque					
	gap	*bridge*	*stator*	$U_{1ph\ rms}$	*THD*	*T[Nm]*[a]
IPM-111	1.0	0.5	M250-35A	360.3	0.49	918.0
IPM-112	1.0	0.5	Arnon-5	367.7	1.40	1050.5
HAPM-111	1.0	2.0	M250-35A	268.8	0.33	1002.4
HAPM-112	1.0	2.0	Arnon-5	269.4	0.34	1103.8
IPM-121	1.0	1.5	M250-35A	251.5	0.43	722.9
IPM-211	3.0	0.5	M250-35A	229.2	0.17	799.1
IPM-221	3.0	1.5	M250-35A	155.8	0.19	623.4

The table shows the reduction of the induced voltage and harmonics due to the increase of the air gap or the strengthening of the rotor design, while the data are limited as it does not show the reference data of the rotor strength calculations.

4.2 Reconfigurable Machine Winding

For simplicity, the operating speed of the LP shaft generator can be divided between ground and flight mode, which is *1500* and *7500 rpm*, respectively. The following calculation example is given, in which a *PMSM* with six parallel coils and *28 turns* is reconfigured into three parallel paths, two coils in series.

The phase current and DC-link voltage remain the same, which is *600 Arms* and *750 V*, respectively. The terminal power of two different winding configurations, 6 parallel and 3 parallel paths, is shown in Figure 18. The total losses, which includes core losses and winding DC losses are shown Figure 19, where coil currents are *100 Arms* and *200 Arms*, respectively. The winding losses are calculated at *120°C* and permanent magnet (*PM*), which is *N30UH*, temperature is chosen at *60°C*. The power extraction capability at *1500* and *2000 rpm* is *83* and *117 kW* and result in power losses of *20* and *24 kW* and an efficiency of *80.4* and *83.2%*.

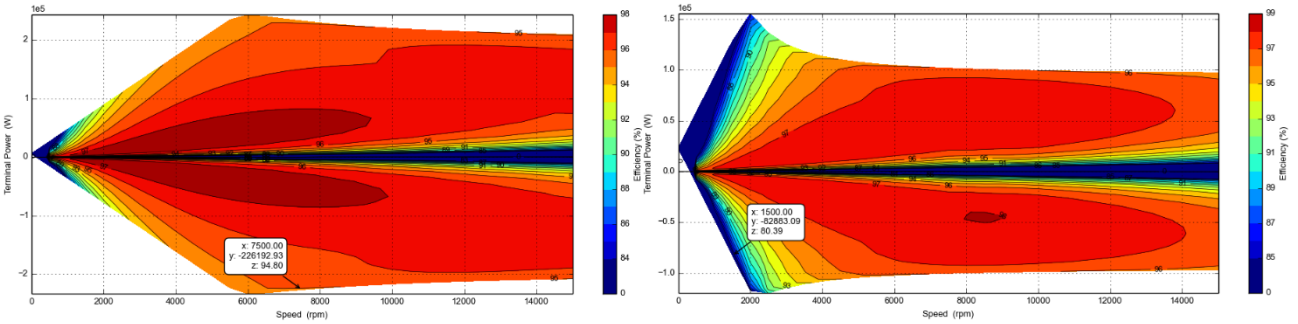

Figure 18 – Efficiency map as a function of terminal power and rotation speed with 6 (left) and 3 (right) parallel connected coils per phase

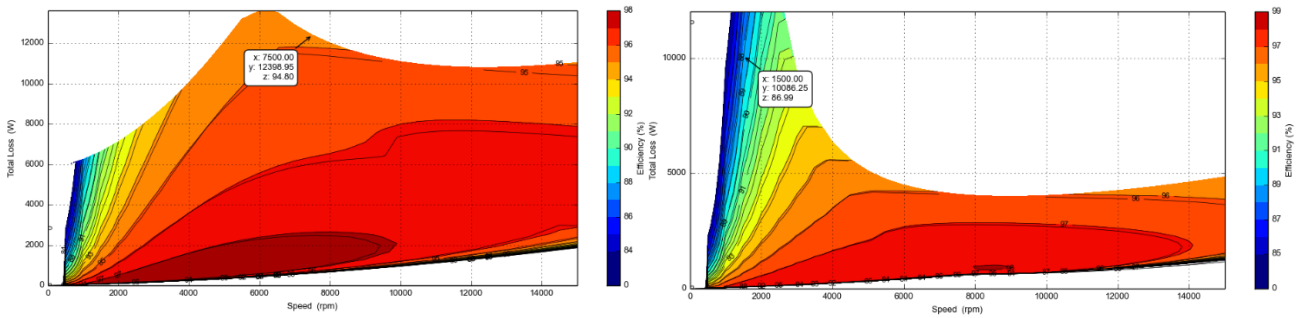

Figure 19 – Total losses of the PMSM with 6 (left) and 3 (right) parallel connected coils per phase

Ansys Motor-CAD v14.1.7 is used to estimate the PMSM characteristics. The machine is configured according to IPM-221 (Table 2) and the main difference is that a slightly stronger PM and *Arnon-7* are used. The reference torque of *648.7 Nm* is calculated and at *2000 rpm*, which is the starting point for the field weakening (WF) region.

Based on model-based studies, the following observations are made:

- High torque density, and the associated power density, must be reduced by increasing the magnetic air gap to maintain higher efficiency over a wide speed range.
- If the power output of the generator is required at both low and high speeds, then switching the windings is one of the ways to achieve this, but at the expense of higher losses.
- To increase heat transfer, the complex problem of increasing the number of parallel cooling channels and reducing AC losses must be solved simultaneously, where a cross transposition technique [22] is one of the possible ways to find solutions.

4.3 Machinette

Just as the modularity of electrical drive components increases the possibility the system to be flexibly and sustainably operated, so is a developable and researchable experiment that enables immediate monitoring of component performance, rational production, and assembly challenges. The stator integration evaluation platform, a stator segment of a *12-pole 18-slot* machine [10], is shown on the right in Figure 3 and the aim is to study manufacturing and assembling effects, selection of coolant, power losses at different loading conditions and resulting temperatures. The concern of induced losses in the winding and unforeseeable core losses due to manufacturing are

some of aspects when designing the experiment. Calculations of core losses are often inaccurate, and the differences are due to both the magnetic load and the way the steel sheets are treated, cut, and assembled.

To find out the different effects, a co-simulation model has been developed for the elementary part of the stator. As an example, a 2D detail view of the stator tooth and slot is shown (Figure 20) showing the cross-section of the winding, with a distribution of flux and current density and a distribution of temperature. In heat transfer calculations, cooling channel temperatures are used to calculate the advection in the channel. In addition to the cooling area of the winding, the stator jacket cooling is also used.

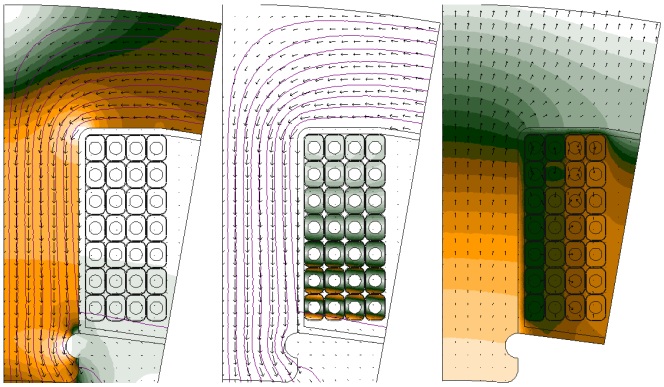

Figure 20 – Distribution of flux density (left), current density (middle) and temperature (right) of the stator elementary section

For the sake of simplification, color scales and values have not been added to Figure 20 because the purpose of the calculation program is to record the load curve at the nominal operating point of *7500 rpm* and to define the cooling conditions. The purpose of the model-based experiment is to design a machinette, an elementary section of machine, that purpose is more precisely account the effect of slot leakage and AC losses.

5. Electrical Machine to Turbo Engine Interactions

To study the interaction between the electric machine and the turbocharged engine, the structure of the system in terms of the transmission of the turbo engine shafts and electric machines is first examined. Thereafter, the questions are what the electric drive-based tests are. And finally, turbo-engine model-based research.

5.1 Turbine Engines with Electrical Machines

Electrical machines inside or in close proximity to the turbine and documentation of their practical performance and challenges are relatively limited. When looking at a multi-spool gas turbine powertrain [23]-[27] then the main preference of power interaction between the spools are by the driveshaft. However, if the faultlessness of the electrical machine (reluctance machine), and the power-to-weight ratio, allow them to be internally embedded inside the engine of the gas flow components [22], this would certainly be an advantage if it provides more maintenance free solutions. Apart from power take of solutions there is a particular interest of mechanical integration and not least various gearbox solutions [28][29]. The main interest here is, in fact, how the HPS electrical machine is connected to the turbine to explore the benefits of system benefits and development options when more specific system component models, such as the LPS machine, are added to the system model.

5.2 Electric Drives Testing

For example, the most common way to test LPS and HPS machines back-to-back, assuming they have the same rated power, is to connect them to a rated speed via transmission. This testing is likely to lead to several practical challenges related to power electronic control of safe energy management. Considering electrical machine to turbo engine interactions the concern is more on electromechanical interactions [30][31] not least ripple and failure modes.

5.3 Gas Turbine Model Based Exploration

Implementing electric machinery offers another level of possibilities for controlling the engine beyond the firing per se and variable geometry for the compressors. A geared turbofan engine is an enabler for integrating electric machinery without going through the auxiliary gearbox. This feature offers several levels of freedom, e.g., frequencies, voltage turn-down, etc. During high engine loads, the transferred energy flows within the engine are massive, and the input from having the mentioned machines are relatively minute. The way to assess the engine performance is by using a cycle deck for calculating the engine matching where the code finds possible engine operational points. This type of calculation is based on component characteristics such as the compressor- and turbine maps, pressure drops in ducts and the combustion system, mechanical losses, etc. The work presented here is based on the GKN technology carrier *RM400* used for notional engine concept studies. This engine model represents state-of-the-art geared turbofan engine technology for future aircraft. In a normal case, without the possibility of transferring power from the high-pressure shaft to the low-pressure shaft (and vice versa), the load distribution is largely set by the available, total engine pressure ratio and the low-pressure turbine swallowing capacity. The former is largely a function of the compression system, firing, and the swallowing capacity for the first turbine. A full discussion is outside the scope in the current text, and the reader is referred to the open literature on the subject. In the current work, several low-load conditions have been analyzed for assessing the potential from the extra level of freedom. One such is ground idle, where the engine is fired at some minimum point. This should be as low as possible to reduce the fuel consumption, the applied brake force but also the core engine exhaust temperature. In this case, the electric machinery offers the possibility of reducing the exhaust temperature. The cycle work has been carried out by using the GasTurb performance deck version 13 by Dr. Kurzke [32] and version 14.

6. Conclusions

This article devotes to the components of an electrical machine for their prototyping and introductory testing to obtain better input data for determining not only the characteristics of an electric machine but also refine the design for manufacturing approach. This electrical machine has direct-cooled winding including stator housing cooling and is designed for a geared turbofan directly connected to low pressure shaft. To get a clearer picture, the article looks into system and part-system evaluation aspects to obtain better understand the design specifications and conditions presented to the machine.

Experiment-based work performance is limited by technical constrains and the resulting conclusions are:

- Two different fabrication methods have been chosen for the production of the 28-turn coil: 1) a stepwise transition of the end turn in crossover section, and 2) a smooth and compressed transition of the end turn in crossover section. The main concern on the manufacture of coils is not the backlash or the displacement due to reaction forces, but the control of of the forces applied to form the turns and the natural or easily formed direction of the materials. This leads to inaccuracies and cumulative discrepancies. However, the oversize of a practically made winding is below the permissible limits, but it provides important practical experience for better quality winding.
- The assessment of cooling capacity is mainly limited to existing low-pressure test systems used for forced air and oil cooling tests. The water-cooled test is limited to recording the hydraulic characteristics at low pressure (less than *5 bar*). The disadvantage also limits the visibility of the actual pressure in the prototype winding. In the absence of experimental data, it is not possible to say with certainty how well water or electric hydraulic cooling oils work but due to the availability of high pressure pumps that allow for pressure (above *100 bar*) and flowrate (above *2 L/min*) requirements, it gives confidence that the answer is nut just purely theoretical.

Model-based conclusions are:

- Even if the theoretical design of an electrical machine allows the characteristics of the machine over a wide speed range (Figure 18), it is unlikely that the electric machine will in fact

provide as wide high efficiency range. Specific estimation models for calculating AC losses must complement the overestimated efficiency.

- Switching the stator winding allows a little more to load the machine at lower speeds, but the increase in power is so small that it could be of practical interest.

7. Contact Author Email Address

mailto: avo.reinap@iea.lth.se

8. Copyright Statement

References

[1] Wang, Y. Nuzzo, S. Zhang, H. Zhao, W. Gerada, C. Galea, M. "*Challenges and Opportunities for Wound Field Synchronous Generators in Future More Electric Aircraft*", IEEE Transactions on Transportation Electrification, V 6 n 4, 2020, pp.1466-1477

[2] Secunde, R. R. Macosko, R. P. Repas, D. S., "*Integrated engine-generator concept for aircraft electric secondary power*", NASA Technical Memorandum, V n X-2579, June 1972, pp.

[3] C. A. Ferreira, Richter, E., "*Detailed Design of a 250-kW Switched Reluctance Starter/Generator for an Aircraft Engine*", SAE Transactions, V 102, 1993, pp.289-300

[4] Radun, A. Richter, E., "*A Detailed Power Inverter Design for a 250 kW Switched Reluctance Aircraft Engine Starter/Generator*", SAE Transactions, V 102, 1993, pp.274-28

[5] Richter, E., Ferreira, C. "*Performance evaluation of a 250 kW switched reluctance starter generator*", IAS '95. Conference Record of the 1995 IEEE Industry Applications Conference Thirtieth IAS Annual Meeting, Oct 1995, pp.434-440 vol.1

[6] Mitcham, A. J., Grum, N. "*An integrated LP shaft generator for the more electric aircraft*", IEE Colloquium on All Electric Aircraft (Digest No. 1998/260), June 1998, pp.8/1-8/9

[7] Mitcham, A. J. J. Cullen, J. A. "*Permanent magnet generator options for the More Electric Aircraft*", 2002 International Conference on Power Electronics, Machines and Drives (Conf. Publ. No. 487), June 2002, pp.241-245

[8] Sun, Z., Ede, J. D., Wang, J., Jewell, G. W., Cullen, J. J. A., Mitcham, A. J., "*Testing of a 250-Kilowatt Fault-Tolerant Permanent Magnet Power Generation System for Large Civil Aeroengines*", Journal of Propulsion and Power, V 24 n 2, 2008, pp.330-335

[9] Bird, J. Z. "*A Review of Electric Aircraft Drivetrain Motor Technology*," in *IEEE Transactions on Magnetics*, vol. 58, no. 2, pp. 1-8, Feb. 2022, Art no. 8201108, doi: 10.1109/TMAG.2021.3081719.

[10] Reinap, A. "*Aerospace Electric Generator Design Considerations*," 2019 9th International Electric Drives Production Conference (EDPC), 2019, doi: 10.1109/EDPC48408.2019.9011859

[11] Sugden, G. B. "*Oil-cooled a.c. generators for aircraft – present trends*", Students' Quarterly Journal, V 40 n 160, June 1970, pp.128-133

[12] Guo, Y. Lu, C. Hua, L. Zhang, X. "*Optimal Design of High-Power Medium-Frequency Transformer Using Hollow Conductors with Consideration of Multi-Objective Parameters*," Energies, 2020. 13(14):3654. doi: 10.3390/en13143654

[13] Luvata White Paper, "*Luvata hollow conductors – enabling more efficient electric vehicles with direct stator cooling*", luvata.com

[14] Nitche, E. Naderer, M. "*Internally cooled hollow wires doubling the power density of electric motors*", ATZ elektronik worldwide, pp. 42-47

[15] Petrov, I. Lindh, P. Niemelä, M. Scherman, E. Wallmark, O. Pyrhönen, J. "*Investigation of a Direct Liquid Cooling System in a Permanent Magnet Synchronous Machine*," in *IEEE Transactions on Energy Conversion*, vol. 35, no. 2, pp. 808-817, June 2020, doi: 10.1109/TEC.2019.2952431.

[16] Cai, W. Fulton, D. "*Multi-Phase Fractional Slot Windings for Electric Machines Having Segmented Bar-Shaped Windings*", US Patent 7348705 B2 Mar. 25, 2008

[17] Neet, K.E. "*Automotive Alternator Stator Assembly with Rectangular Continuous Wire*" US Patent 6750581 B2, Jun. 15, 2004

[18] Reinap, A. Andersson, M. F. Márquez-Fernández, J. Abrahamsson, P. Alaküla, M. "*Performance Estimation of a Traction Machine with Direct Cooled Hairpin Winding*," *2019 IEEE Transportation Electrification Conference and Expo (ITEC)*, 2019, pp. 1-6, doi: 10.1109/ITEC.2019.8790545.

[19] Hagedorn, J., Sell-Le Blanc, F., Fleischer, J., "*Handbook of coil winding. Technologies for efficient electrical wound products and their automated production*", Springer Vieveg 2018, ISBN 978-3-662-54401-3

[20] Reinap, A. Gabassi, M., Alaküla, M., Andersson, M., "*Assessment of cooling integration with direct cooled windings*," 2018 IEEE International Conference on Electrical Systems for Aircraft, Railway, Ship Propulsion and Road Vehicles & International Transportation Electrification Conference (ESARS-ITEC), Nottingham, UK, 2018, pp. 1-6. doi: 10.1109/ESARS-ITEC.2018.8607655

[21] Reinap, A. "*Aerospace electric generator specification and selection – opportunities and challenges*", Aerospace Technology Congress, 8-9 October 2019, Stockholm, Sweden

[22] Reddy, P. B. Jahns, T. M. Bohn, T. P., "*Transposition effects on bundle proximity losses in high-speed PM machines*," *2009 IEEE Energy Conversion Congress and Exposition*, 2009, pp. 1919-1926, doi: 10.1109/ECCE.2009.5316037.

[23] Hield, P. M. Cundy, J. M. Midgley, R. A. Newton, A. C. Rowe, A. L. "*Shaft power transfer in gas turbine engines with machines operable as generators or motors* ", US5694765A, Dec 1997

[24] Coles, J. R. Holme, M. Doyle, J. P. "*Electrical generator an aero-engine including such a generator, and*

an aircraft including such a generator", US6894417B2, Oct 2002

[25]Gaines, L. T. Auer, P. J. Lane, G. H. Wissinger, J. A. "*More electric aircraft starter-generator multi-speed transmission system* ", US7481062B2, Jan 2009

[26]Eick, C. D. Gaines, L. T. Laidlaw, M. J. Benson, D. M. Portolese, L. A. Flaherty, B. L. Pearson, W. T. "*More electric aircraft power transfer systems and methods*", US7552582B2, Jun 2009

[27]Jones, S. R. Southwick, R. D. "*Turbine engine transient power extraction system and method* ", EP1947311A2, July 2008

[28]Lemmers JR, G. C. Behling, D. S. "*High to low pressure spool summing gearbox for accessory power extraction and electric start*", US7882691B2, Feb 2011

[29]H. Huang, J. Zywot, "*Accessory gearbox with a starter/generator*", US8857192B2, Oct 2014

[30]Feehally, T. Damián, I. E. Apsley, J. M. "*Analysis of Electromechanical Interaction in Aircraft Generator Systems*", IEEE Transactions on Industry Applications, V 52 n 5, Sep. 2016, pp.4327-4336

[31]Ahumada,C. Garvey,S. Yang, T. Kulsangcharoen, P. P Wheeler,. Morvan, H. "*Minimization of electro-mechanical interaction with posicast strategies for more-electric aircraft applications*", IECON 2016 - 42nd Annual Conference of the IEEE Industrial Electronics Society, Oct 2016, pp.4423-4428 [7794134]

[32]Kurzke, Joachim. "*Design and off-design performance of gas turbines*." Gasturb 13 Manual (2018).